SAND77-0701
Unlimited Release
Vol. 3, No. 1

SANDIA TECHNOLOGY

SF 2900 QAB(6 - 75)

SAND77-0701
Vol. 3, No. 1

SANDIA TECHNOLOGY

Sandia Laboratories

March 1977

J. A. Mogford, *Technical Editor*
W. L. Garner, *General Editor*

FOREWORD

Sandia Laboratories is a multiprogram laboratory operated for the Energy Research and Development Administration. Our primary responsibilities are in research and development for nuclear weapon systems. Substantial efforts are also applied to energy research and other programs of national importance. This publication describes some of our developments and accomplishments in unclassified programs. Activities of classified nature are reported in a companion publication, Sandia Technical Review.

This facility will provide a safe and environmentally acceptable disposal for radioactive wastes that have resulted from the national defense effort.

A radioactive-waste isolation pilot plant

The objective of the Waste Isolation Pilot Plant (WIPP) program is to demonstrate the suitability of bedded salt — specifically, the bedded salt deposits in the Los Medaños area of southeastern New Mexico — as a disposal medium for radioactive wastes. Our program responsibilities include site selection considerations, all aspects of design and development, technical guidance of facility operation, environmental impact assessment, and technical support to ERDA for developing public understanding of the facility.

The principal justification for the WIPP is the need for storing wastes generated by the national defense program over the past 30 years. These wastes vary in content of elements heavier than uranium (TRansUranics — TRU) and in level of radioactivity. Materials (such as clothing, wood, wipe rags, scrap tools, etc), contaminated with transuranics but low enough in radioactivity to permit "contact" handling, are called TRU wastes. Other wastes, which may contain transuranics but require remote handling because they contain fission products, are subdivided into intermediate- or high-level wastes (ILW or HLW). Although these subcategories are not sharply distinguished, it is generally true that HLW has a thermal output requiring special consideration for salt storage, while ILW poses only the radiation problem.

Currently in temporary storage at various ERDA facilities are about 100,000 m^3 of TRU wastes, and HLW equivalent to about 60,000 m^3 when processed to solids. A relatively small volume of ILW exists in the form of high-radioactivity TRU waste, obsolete process vessels, etc. In addition, TRU wastes are being generated at a rate of about 6000 m^3 per year. As a pilot plant, the facility will receive only TRU wastes and ILW generated by the government. However, the design is also compatible with the radiation and thermal characteristics of commercial high-level wastes, and experiments to define the behavior of HLW in salt storage will begin as soon as underground construction permits. Our present charter calls for recovering the HLW upon completion of the experiments and moving it to a licensed HLW repository.

As the laboratory responsible for developing a WIPP for existing wastes, we consider ourselves neither proponents nor adversaries of a nuclear fuel cycle or even bedded-salt storage but rather technical managers of a pilot program that could demonstrate the feasibility of long-term nuclear waste disposal in salt formations.

Site Selection

In selecting a site for long-term storage of radioactive nuclear wastes we seek to satisfy two fundamental objectives:

> The radioactive materials should be kept from interacting with the biosphere until sufficient dilution or decay of the radioactivity has occurred — a time span that depends on many factors but is sometimes considered to be about 10 half-lives of the radionuclide.*
>
> The dedication of a site to repository use should produce the least possible conflict with other human endeavors.

From these objectives are derived a number of criteria (pertaining to, for example, geology, hydrology, seismology, demography, etc) that must be satisfied by a site. Our program includes investigations to ascertain as

*Some radionuclides do not require long-term storage: e.g., ^{131}I has a half-life of about 8 days and ^{198}Au about 3 days. Long-lived nuclides such as ^{90}SR (half-life ≈28 yrs) and ^{137}Cs (half-life ≈30 yrs) require safe storage for hundreds of years. Still longer storage times are required for extremely long-lived radionuclides as, for example, ^{239}Pu with a half-life of about 24,000 years.

For further information about this article contact W. D. Weart.

completely as possible that the specific site fulfills the selection criteria.

To be considered for a site, an area must first possess the proper geology: e.g., salt beds with appropriate thickness, extent, depth, and absence of moving water. Geological investigations, among the most important for a specific site, evaluate potential conflicts with mineral resource exploitation and possible ways waste could be released by natural phenomena during the long-term storage that would follow if the WIPP should be converted to a repository. Geologic evidence also provides some indications of past climatic conditions and hence of possible long-term future environmental changes in the region.

Hydrologic investigations are of primary importance for a pilot plant that might become a repository since all credible modes of release of radioactivity from a repository involve, at some stage, transport by ground water. These investigations consist of thorough evaluation of existing and potential aquifers to determine possible routes of ground water flow that might carry radionuclides to the biosphere.

Seismological studies assess the earthquake risk to the WIPP by analysis of the seismic history of the area. This analysis, together with geologic studies will be used in assessing the long-term potential for faulting, folding, or other deformation of the earth's crust.

The site under consideration is in southeast New Mexico about 50 km east of Carlsbad (Fig. 1). A surface facility

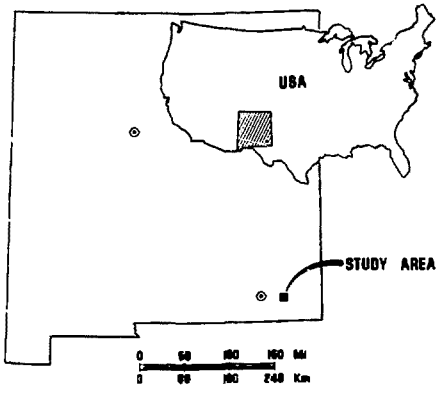

Fig. 1 The site being considered for construction of a waste isolation pilot plant is in southeast New Mexico.

of about 0.25 km^2 (60 acres) will be fenced and protected. The repository, an underground area of 7.8 km^2, will be surrounded by two control zones, each 1.6 km wide. The total area used or controlled by the pilot plant will be $\approx$ 75 km^2. All of the land is owned either by the federal government or by the State of New Mexico. The area, which is unoccupied, is presently used for grazing at a density of about 9 cattle per section, or one head per 70 acres.

The possibility that some resources may be excluded as potential supplies is being thoroughly investigated. We have completed a drilling program, in conjunction with the U. S. Geological Survey, to evaluate potash resources in the area. Independent petroleum engineering concerns have been retained to evaluate oil and gas availability beneath the potential site and to assess the economics of recovering the resources. In addition, we are investigating techniques for recovering oil, gas, and potash without jeopardizing the security of the site.

WIPP Design

A policy which significantly influences the pilot plant concept is ERDA's commitment to provide for and demonstrate retrievability of waste during the pilot plant stage. The HLW experiments present the most severe retrieval problem because of the thermal and radiation effects on the salt and on the waste package. Some emplacement experiments imply retrieval by simply overcoring the waste — in effect recovering a "salt cannister" containing the waste.

WIPP waste acceptance criteria require that all wastes be in solid form. To the extent practicable, TRU wastes will be incinerated, stabilized in concrete or glass, and packaged in 200-liter drums or larger-volume boxes. Liquid HLW will be calcined to a dry powder, stabilized in a low leachability solid such as borosilicate glass, and packaged in stainless-steel canisters about 30 to 40 cm in diameter and 3 to 4.5 m in length. ILW processing and packaging will be chosen to accommodate the specific waste type.

Only the TRU wastes are amenable to handling by contact methods; all other waste types require shielding and/or remote handling. Therefore the WIPP will be divided into a "cold facility" for TRU wastes and a "hot facility" for all other wastes. Our repository design (Fig. 2) has two storage levels at depths of about 650 m and 800 m. They are served by a man-and-materials shaft

which is isolated from the HLW storage by airlocks. The two areas have independent ventilation systems and separate waste transport shafts which link the levels to self-contained surface facilities whose interiors are isolated from the outside atmosphere. Each surface facility can receive wastes by rail or motor truck. Provision for decontaminating shipping casks and waste containers, and facilities for "overpacking" ruptured waste packages will be necessary. Except for treatment of site-generated decontamination wastes and air filters, no other waste processing will be carried out at the WIPP.

Supporting Studies

Theoretical, laboratory, and field studies are necessary to ensure safety and effectiveness of the pilot plant design and operation, and to answer basic questions regarding confinement of radionuclides. The investigations planned or in progress are categorized as Fundamental Studies (which precede establishment of a pilot plant in bedded salt) and as Design and Operational Studies (which may continue throughout the life of the plant).

Fundamental studies include investigations of rock mechanics, computer analyses of mine designs, chemical and physical characterization of waste, and geochemical analyses of the waste-cannister-salt system. Experimentally determined thermal and mechanical properties of rocks are being used in temperature-dependent structural studies that will influence placement of repository cannisters, room size, pillar dimensions, and other design parameters.

Investigations pertaining to the design and operation of the WIPP include in-situ stress and rock deformability

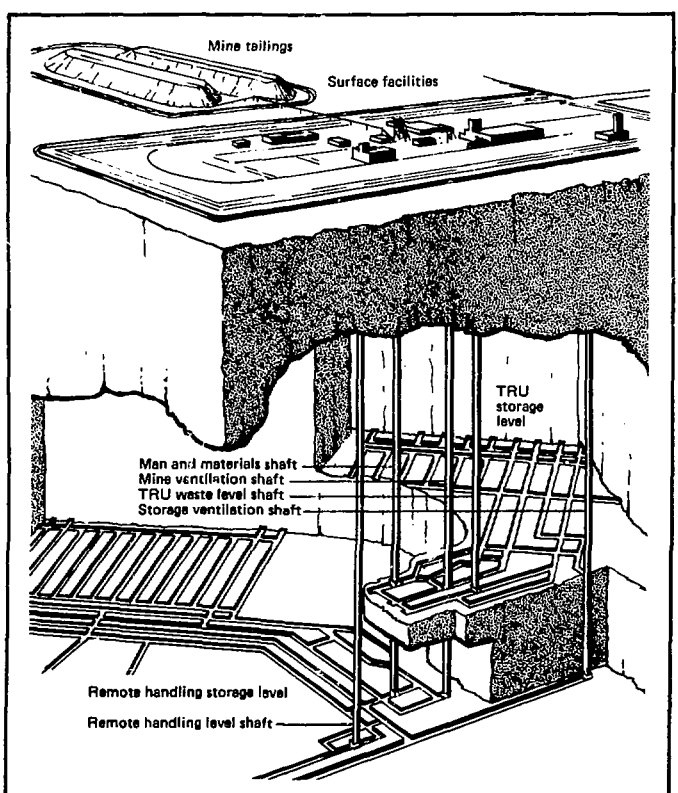

Fig. 2 The waste isolation pilot plant is a bi-level facility with storage at depths of 650 and 800 metres. Transuranic (TRU) -contaminated wastes that can be contact handled are stored on the upper level; intermediate- and high-level wastes requiring remote handling are stored on the lower level.

measurements, pillar model experiments, structural integrity evaluations, and material/salt interactions. We plan to make measurements, through bore holes, of the rock deformation (creep) at mine depths to learn how rapidly openings will close. Spontaneous closure is obviously desirable for long-term storage, but premature closure will complicate retrievals.

Environmental Impact Considerations

We are preparing a Draft Environmental Impact Statement (DEIS) which sets forth possible impacts of the WIPP on the natural environment. We have established that the ongoing geologic processes pertaining to this site will not destroy the integrity of the repository during the next few hundred thousand years. Currently under thorough investigation are the potential consequences of inadvertent human penetration of the repository. Catastrophic events, such as meteor impact or breaching of the salt beds by major faulting, are among the improbable occurrences that are being considered. The DEIS also addresses the social and economic impacts of the WIPP.

The completed Draft Environmental Impact Statement will be distributed to government agencies, environmental organizations, and individuals for comment. Public hearings on the facility and its impact will be held in several localities to assure that the public participates in the deliberations. An acceptable statement of environmental impact is an essential step in the development of the WIPP.

The Future

The Conceptual Design Report and the Draft Environmental Impact Statement, both to be completed and forwarded to ERDA in June 1977, are prerequisites to receiving authorization to start construction in 1979. First receipt of low-level radio-active waste is anticipated in 1983 and in that year we will also begin experiments with high-level waste. The eventual scope and operational lifetime of this repository will depend upon the availability of other geologic disposal sites now being investigated and upon new disposal technologies now under study. If necessary, this one site could accommodate all defense and commercial radioactive waste generated in the United States into the 21st Century.

40,000 rpm spin facility

Field firing of nuclear artillery shells has indicated that failures could be caused not only by the violent setback force of the explosive launch but also by the centrifugal force of the spin imparted by the gun barrel's rifling. To reduce the cost and time for obtaining test data from field launches, we now simulate the spin portion of the flight environment in a test facility capable of spinning a 350-kg test specimen up to 40,000 rpm.

Entire shells, suspended vertically from a flexible support in a 1.2-m-diameter concrete-lined pit, are spun at typical launch conditions of 10,000 to 20,000 rpm. The arming and fuzing sequence for the shell, including detonation of small explosive devices, can be carried out during spin. Slip rings are available for sending signals to test devices inside the shell and for gathering performance data during the spin operation. The test chamber can be evacuated to prevent the excitation of vibration modes not present in free flight, and the test unit can be temperature-conditioned with a portable temperature-control unit.

Tests of artillery shells in actual firings rely heavily on telemetered data returns. Use of the spin facility to make fast, inexpensive, preflight tests of telemetry components has done much to prevent data-loss failures in field tests.

Recently an additional application for the facility has been found in one of our energy programs. Composite fly wheels, being studied as energy storage devices, are tested on the spinner up to its limit of 40,000 rpm.

For further information about this article contact R. M. Hargreaves.

We are developing a nuclear thermal flashblindness protection device that satisfies a Required Operational Capability for the Strategic Air Command.

Nuclear thermal and flashblindness protection for air crews

Strategic and defensive missions of the U. S. Air Force could be seriously hampered if air crews were temporarily blinded by the intense visible and thermal radiation from nuclear detonations. To protect against such disablements, we are developing a thermal flashblindness protection device (TFPD) for that service. Protection is afforded by an electrically controlled solid-state shutter lens in a goggle assembly (Fig. 1). The lens, a thin wafer of transparent electro-optic ceramic sandwiched between crossed polarizers, reacts to a light pulse in microseconds, reducing transmitted light sufficiently to prevent flashblindness.

The key to protection is a transparent ceramic material, an outgrowth of ferroelectric ceramics development for nuclear weapons. This material evolved as a result of our discoveries of process techniques and controls required to produce the chemical and mechanical microscopic perfection necessary to achieve optical transparency in ceramics of this type.

The TFPD is being readied for initial production in late 1977. The production process involves transfer of new technologies to manufacturers of several goggle subassemblies. The Bendix Corporation, Kansas City Division, an integrated contractor to ERDA, will not only produce the remaining subassemblies but will also assemble the complete device.

Fig. 1. *Prototype of helmet-mounted goggle.* **An electrically controlled solid-state shutter reacts to a light pulse to provide protection from thermal and flashblindness.**

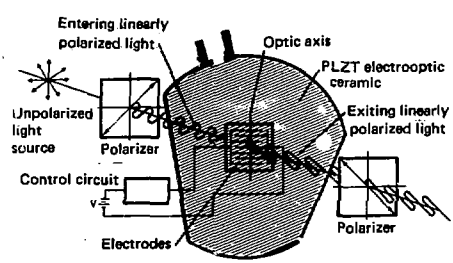

Fig. 2. **Schematic of an electro-optic shutter in the open state. The PLZT goggle-lens element (over the center part of the schematic) demonstrates the transparency of the element and shows the line-electrode pattern.**

Operating Principle of the Goggle Device

The electro-optic ceramic is one member of a family of compositions of lead zirconate titanates with substitutions of lanthanum; it is called PLZT for lead-lanthanum-zirconate titanate. The X/65/35 PLZT ceramic materials (lead zirconate/lead titanate ratio of

For further information about this article contact P. D. Wilcox.

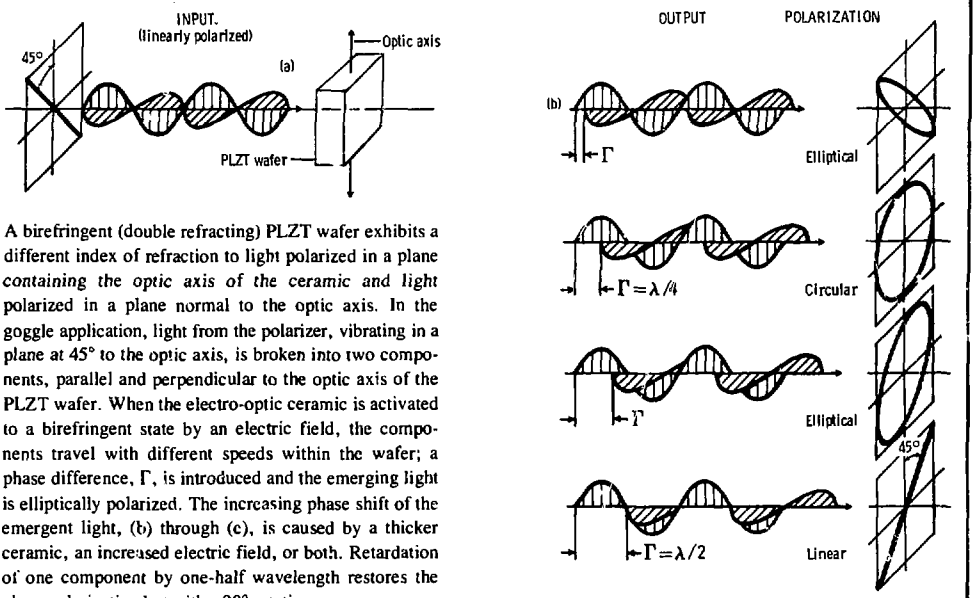

A birefringent (double refracting) PLZT wafer exhibits a different index of refraction to light polarized in a plane containing the optic axis of the ceramic and light polarized in a plane normal to the optic axis. In the goggle application, light from the polarizer, vibrating in a plane at 45° to the optic axis, is broken into two components, parallel and perpendicular to the optic axis of the PLZT wafer. When the electro-optic ceramic is activated to a birefringent state by an electric field, the components travel with different speeds within the wafer; a phase difference, Γ, is introduced and the emerging light is elliptically polarized. The increasing phase shift of the emergent light, (b) through (c), is caused by a thicker ceramic, an increased electric field, or both. Retardation of one component by one-half wavelength restores the plane polarization but with a 90° rotation.

65/35, with X atomic percent of the lead replaced with lanthanum) with X typically greater than 9, exhibit electrically controlled uniaxial birefringence (see box), whose magnitude varies with the square of the electric field. Thus, polished and electroded PLZT wafers, properly oriented and sandwiched between crossed polarizers, create a light modulator in the configuration of an electro-optic shutter, called a Kerr cell (Fig. 2).

Varying the voltage applied to the electrodes on the surface of the PLZT wafer changes the optical properties of the wafer and causes the shutter to open or close. In the zero-voltage condition, or "closed" state, the PLZT material is optically isotropic; therefore the plane of the light polarization is unaffected and the crossed polarizer pair efficiently blocks the light transmission. When voltage is applied to the PLZT it becomes optically birefringent, causing the linearly polarized light which passes through it to change to some state of elliptical polarization. A component of this light will pass through the second polarizer, producing the "open" state of the Kerr cell. If the applied voltage exactly matches the half-wave voltage* of the PLZT wafer, the light which leaves the wafer will again be linearly polarized, but with its polarization orthogonal to that of the entering light. Consequently, maximum light intensity will be admitted through the second polarizer. This is the "fully-open" state.

Transmittance in the fully open state is about 20%, roughly equivalent to the transmittance of pale polaroid sunglasses. The transmittance is limited only by losses in reflection at interfaces and by a small amount of absorption and scattering in the polarizers themselves. In the closed state, transmittance is reduced nearly four orders of magnitude to 0.003%. By means of electrical control, transmittance can also be varied continuously over the entire on-to-off range.

A special glass filter (KG-3), that is transparent to visible radiation, is used in front of the first polarizer to absorb the infrared (thermal) radiation from the nuclear burst. Transmittance in the ultraviolet is always blocked, since both the PLZT and the polarizers are opaque to radiation below about 370 nm in wavelength.

*That voltage at which the PLZT wafer will shift the phase relationship of two components of the light by one-half wave length.

The Optical Lens Assembly

The lens assembly, a key element of the goggle device, is based on the availability of transparent electro-optic ceramics and the development of new technologies including ceramic fabrication, polishing of large thin ceramics, production of long, continuous, line-electrodes (Fig. 2), and assembly lamination.

Ceramics: A new level of physical and chemical perfection was required to produce the transparency of the polycrystalline ceramic. The physical defects, including pores, are so few that light scattering is not observed as it is in conventional polycrystalline ceramic materials. Also, chemical homogeneity is maintained so thoroughly that local changes in birefringence do not interfere either with transparency or with optical applications.

Polishing operations on 0.4-mm-thick, 102-mm-diameter polycrystalline wafers require considerable care and cleanliness, and must contend with such difficulties as grain pull-out, differential polishing rates of individual grains, and stresses that create birefringence and degrade the shutter or cause warping of the thin wafers.

Electroding by the photo-lithographic method, widely used in the electronics industry, is not satisfactory because of yield deficiencies. A new technology has been developed for producing electrodes (which are 75-μm wide, several meters in length, and completely free of breaks) on each side of a polished wafer without creating surface stresses or damage.

Lamination of several elements to form the assembly (Fig. 3) requires adhesives with special properties. The adhesives must not only be transparent, rugged, and suitable for production operations, they must also have the correct index of refraction, must not exhibit birefringence when strained or subjected to electric fields, and must not slow the strain release of the ceramic when it is switched to the closed state.

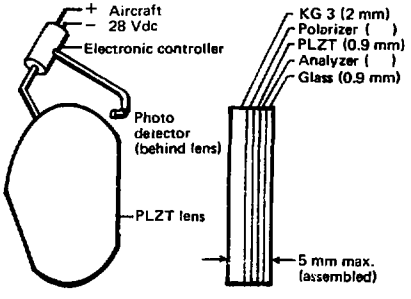

Fig. 3. Photo-optical feedback system and the laminated lens assembly.

Device Design Concepts

The lens assembly is mounted into the goggle frame, which has a silicone skirt along the bottom edge to prevent light leaks (Fig. 1). The goggle connects to the 28 V dc aircraft power through attachments designed to accommodate various goggle positions on helmets of different sizes.

Two photodetectors mounted behind the PLZT lenses monitor ambient light in the forward field of view. Photocurrent generated by ambient light is converted by the controller (Fig. 3) to a voltage that is continuously monitored and stored to represent the ambient light level. All of the ambient light level monitoring, detection, and switching circuitry, except for the photodetectors, is in the controller package along with logic and servo-control circuitry. A dc-dc converter section generates the high voltage (up to 1400 V) required to operate the PLZT lenses. For operation in temperature extremes, a manual control is provided to adjust output voltage and to provide compensation for the temperature-dependent electro-optic characteristics.

Operational Testing

Operational tests were necessary to determine how well aircrews could perform their functions with the limited transmission of the goggles. To confirm operation safety and mission success under these visibility conditions, day and night missions including the pertinent critical flight operations — taxi, take-off, high-level flight, low-level flight, and mid-air refueling — have been flown using operational USAF/SAC aircrews in B-52, KC-135, and FB-111 aircraft. The results of tests with transmission levels of 22% and 16% were almost identical, and the average rating (using the Cooper-Harper method) was "slight to some difficulty, with performance equal to or close to normal." Recommendations from these tests relating to mechanical fit, "rainbow" effects in windscreens, donning and doffing, field-of-view, and weight have been taken into account in the present design.

Solar irrigation experiment

Operation of 160,000 irrigation wells in the Southwest powered by natural gas is threatened by rising prices and eventual fuel shortages. With New Mexico State University we are engaged in a joint experiment (funded by ERDA, the State of New Mexico and the Four Corners Regional Commission) to develop and demonstrate a water-pumping system that uses solar energy as an alternative to natural gas. The near-term objectives are to demonstrate operation of a solar-powered irrigation system based entirely on available technology, and to collect data from temperature sensors, flow indicators, and meteorological instruments that will enable us to thoroughly evaluate the system.

The installation consists of a field of sun-tracking solar collectors, an insulated tank for storing energy as heated fluid, a heat engine, irrigation pump, controls, and a water storage pond. A fluid circulated through the collectors is heated to 490 K and pumped to the thermal storage tank. This fluid is used as needed by transferring its energy through a heat exchanger to a working fluid (freon) which powers a Rankine-cycle engine. The 19-kW (25-shaft-hp) engine will pump 44 L/s (700 gpm) from a 34-m-deep (110-ft) well for 23 hours/day during the 100-day growing season. The water is not applied directly onto a field but is stored in a 5500-m^3 (4.5 ac-ft) pond so that NMSU experimenters can use the water to test irrigation techniques and equipment, and to conduct agricultural experiments. (In normal operation the irrigation water, sufficient for 100 acres of mixed crops, would be pumped directly onto a field.)

The solar irrigation experiment, being installed in the Estancia Valley, near Willard, NM, will be in full operation for the 1977 growing season. When the solar power system is not operating the irrigation pump, it can be used to provide 120-kW-thermal or 19-kW-electrical power for alternative uses.

For further information about this article contact R. L. Alvis

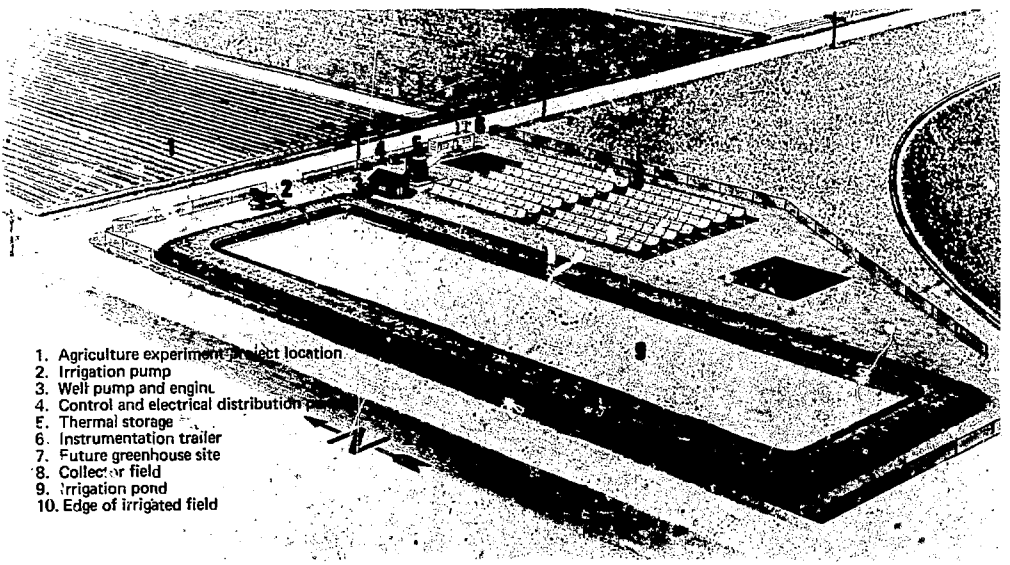

The ERDA/New Mexico solar irrigation experiment will evaluate the technical and economic aspects of an alternative to natural-gas-powered pumps.

A new measurement capability for near-surface analysis is applicable to weapon and energy projects.

Measurement of light-atom distributions in solids

We have developed a sensitive technique that is capable of nondestructively measuring the abundance and depth-distribution of isotopes of hydrogen or helium imbedded in a solid. The measurement is a form of ion-backscattering spectrometry which uses protons to probe within ~10 μm of the surface of a solid. By analyzing the energy of the backscattered protons we can determine the number of atoms of a given mass present at various depths in the target material. This method permits detection of the lightest elements (i.e., those most difficult to detect by conventional ion-backscattering spectrometry) without sacrificing the capability of revealing the abundance and depth-distribution of heavier elements.

This direct measurement technique has made it possible to obtain information that once was either inaccessible or only inferable from related data or theoretical treatments. An important and frequent application of the technique is to studies that use ion implantation to create distributions of light atoms in solids. Ion implantation is a powerful experimental procedure in which a material is bombarded with a beam of ions whose number and energy are varied to alter the abundance and depth-distribution of the ions implanted in the target material. Because we can now directly measure the actual abundances and distributions that result from an implantation, we can accurately define the implant conditions required for a specific desired result. Furthermore, because the measurement is nondestructive, a series of measurements can be made on the same sample to monitor the evolution of a process. For example, we have measured the initial distribution of helium implanted in a metal, then in subsequent measurements kept track of the helium migration.

For further information about this work, contact R. S. Blewer.

Applications

In many situations it is important to measure the distribution of light atoms in a solid, particularly in conjunction with ion implantation when it is used to simulate the atomic distributions that occur in the materials of weapons, energy systems, and microelectronics. Major applications of the technique are found in studies of neutron generator targets and fusion reactor walls.

Neutron generators are used not only in nuclear weapons and in well-logging operations, but also in techniques being developed for cancer treatment. A problem that plagues neutron generators with tritium-impregnated targets is that helium accumulates in the target as the tritium undergoes radioactive decay. When the accumulated helium is eventually released, it will produce free helium in the vacuum tube — and in certain circumstances could produce blistering on the target surface. Because these effects can degrade neutron generator operation, the release phenomenon has been the object of considerable experimental and theoretical investigation. Whereas previous measurements have involved detection of gas that is emitted from the sample,

of the helium-rich layer.

the proton backscattering technique measures directly the helium left in the target. Moreover, it reveals the depth-distribution of helium and other gases in target materials and thus provides a means for developing improved simulations of aged targets.

Subsurface accumulations of helium will also occur in fusion reactor walls that are exposed to the flux of alpha particles (helium nuclei) that are generated by the fusion reaction. These particles, with various energies and incident directions, impinge on the walls and become implanted. If blistering effects like those shown in Fig. 1 occur, they could seriously erode the wall and possibly even quench the power-producing reactions. With our new measurement technique we can measure helium distributions implanted in wall materials, even at elevated temperatures, and can correlate abundances and distributions with the effects they produce.

Proton Backscattering Technique

The scattering of a positively charged particle (in this case a proton) by the electrostatic field of a positively charged nucleus is called Rutherford Scattering.* Rutherford Ion Backscattering Spectrometry (RIBS) is a nondestructive-analysis technique capable of revealing both the abundance and depth-distribution of impurity atoms within the first few micrometers of a solid surface, but until recently, it was thought to be insensitive to low mass atomic distributions of interest to us. RIBS is most useful for detecting heavy impurity atoms in the surface of a material of relatively light atoms because the scattering cross section (the probability that incident atoms will elastically scatter from a target atom) increases as the square of the number of protons in the target nucleus. Thus, with equal atom concentrations of gold atoms in a matrix of aluminum atoms there is a probability of 37:1 that a given incident ion will elastically scatter from a gold atom in the target rather than from an aluminum atom. Although this makes the sensitivity for detection of gold atoms in the target very high, the situation is unfavorable if one is interested in detecting aluminum atoms, and still worse if one wishes to detect even lighter atoms. Our modifications of the RIBS technique permit not only detection of light elements in a solid target but also measurement of their concentration and depth-distribution.

*Named for Lord Rutherford who in 1911 developed a theoretical description of the scattering of charged particles by the electrostatic field of a point charge.

The principles of the proton backscattering technique are schematically illustrated in Fig. 2. A beam of monoenergetic protons is directed at a surface. Most of the protons pass through a thin target essentially without deviation, but some are scattered at large angles by the target atoms. A small silicon detector intercepts the protons backscattered in a given direction, and measures the

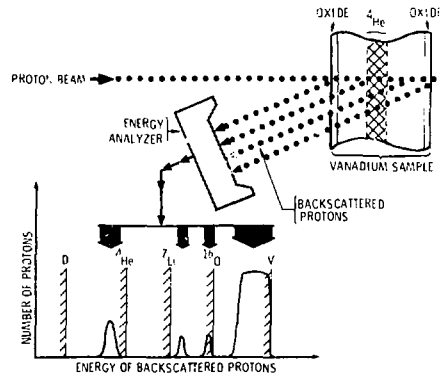

Fig. 2. Schematic of proton backscattering geometry (above) and graph of data showing abundance and depth-distribution of sample constituents (below). The "surface" relative to each element is indicated by the half-hashed lines. The horizontal axis, read from right to left, is proportional to depth for each element.

energy of each. Their energies are determined by (1) the incident proton energy, (2) the scattering angle, (3) the mass of the proton, (4) the mass of the target atom, and (5) the depth in the sample at which the scattering occurs. Since the proton mass and incident energy are known and the scattering angle is selected by the position of the detector, three of the variables are fixed. Thus the measured energy of the backscattered protons is determined by the remaining variables, and its value is different (and unique) for each atom species (element) at a given depth in the sample. The number of protons detected at each energy level is displayed to reveal the number, type, and location of atoms which comprise the specimen.

Measurement sensitivity is increased by selecting the proton energy so that both nuclear and electrostatic forces contribute to the scattering from light atoms, however, the scattering from heavy atoms is caused by electrostatic forces alone. For proton energies of 2 to 3 MeV, nuclear interactions increase the probability of scattering from a hydrogen or helium nucleus by more than two

orders of magnitude. The interaction is still purely elastic, so the scattered protons arrive at the detector with an energy representative of the scattering atom but in much greater quantity than predicted for Rutherford scattering. This scattering enhancement does not occur for the heavier atoms because their stronger electrostatic fields keep the protons from approaching the nuclei close enough to be influenced by the nuclear force. The net effect is a measurement sensitivity that allows us to detect even dilute concentrations of light atoms — for example, ½ atomic percent helium in copper.

Analysis of a vanadium sample is illustrated by the energy spectrum in the lower part of Fig. 2. The distribution of proton energies in the vanadium peak is caused by scattering from vanadium atoms at various depths in the sample. The dual oxygen peaks are readily understood in terms of the energy/depth relationship: the higher energy oxygen peak is produced by scattering from the front-surface oxide, but the peak from the rear-surface oxide is displaced to lower energy because these protons lost energy by traversing the foil sample twice before reaching the detector. Vertical lines are shown at energies corresponding to proton backscattering from different elements in the first atomic layer. The meaurement also demonstrates the absence of other light impurities; for example, no peaks were observed at energies corresponding to deuterium or lithium; therefore these elements were not present in the sample.

Examples

Measurements of the distribution of helium implanted in several metals have provided the first high-resolution validation of calculated helium implant depth and distribution (Fig. 3). A calculation* (solid line) for a helium-implanted titanium sample shows excellent agreement with the experimental data from the multichannel analyzer. The measurement confirms the assumption that the distribution is symmetric about the mean implant depth, and that the distribution was not distorted by diffusion of the implanted gas either toward the surface or deeper into the sample during or after implantation.

Under some conditions, nonsymmetric distributions and gas migration occur in implanted specimens. These effects were clearly evident in experiments conducted for

*See the related article, "A Versatile Computational Capability for Ion-Solid Interactions," in *Sandia Technology*, August 1976 (SAND76-0264).

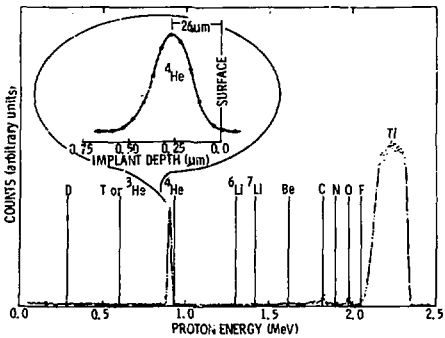

Fig. 3. This spectrum shows the number of protons backscattered with a given energy from a helium implanted foil. The excellent agreement between calculation (line) and analyzer data (points) is shown in the inset.

ERDA's Division of Magnetic Fusion Energy. To simulate the effects of helium bombardment on a hot wall of a fusion reactor, helium was implanted at three elevated temperatures in a vanadium sample (Fig. 4). While the helium distribution is symmetric for the 370 K implant, double peaked distributions have been observed if the implant is made at 670 K. The fraction of implanted gas retained is found to be the same in both cases, although the character of the surface disruption is markedly different. However, if the implant is made at 1070 K, most of the implanted gas is re-emitted without significant surface disruption. The fact that the strongest surface disruption occurs when more than half of the implanted gas is retained, whereas little disruption occurs when most of the gas is released, is at variance with theories which relate surface disruption to gas release. Although these results could be obtained only by measurement, theoretical treatments are now beginning to explain the phenomena in terms of atomistic processes and stress accumulation.

The experiments involving heated vanadium implanted with ions of a single energy showed that different distributions resulted even though the implantation parameters were the same for each sample. The results of experiments using implanted light atoms may depend not solely on the implanted abundances but also on the initial depth-distribution. Specially tailored distributions may be desired to accurately simulate a known distribution or to explore the relationship between distributions and effects. Tailored distributions can be generated by using computer codes to predict the implant energies and fluences that should produce a given distribution and then

by using the proton backscattering technique to determine whether the desired distribution was achieved in a specific sample.

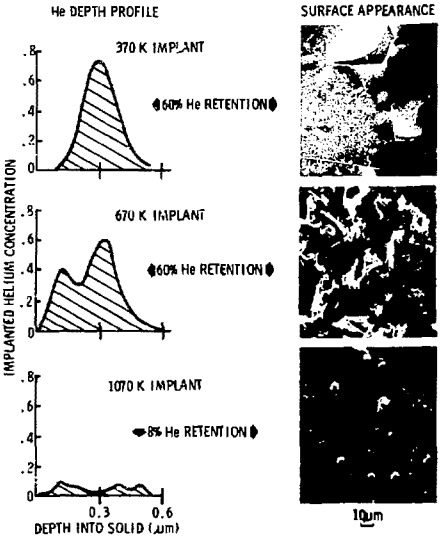

Fig. 4. The proton backscattering technique was used to measure the depth profiles of helium implanted in Vanadium at three elevated temperatures. The effect of the implant on the surface is shown in the photos at right. Helium implantation in hot materials will occur in fusion reactors.

One example of a requirement for a tailored implant distribution is the simulated aging of tritided targets in neutron generators. As a neutron generator ages, the radioactive decay of the tritium produces a uniform distribution of helium in the target. We have computed single energy depositions that combine to produce a distribution uniform within ±5% for a depth of over 0.5 μm (Fig. 5). Samples prepared according to this recipe were measured to determine the actual uniformity achieved, and are being compared with naturally aged samples to determine if the artificially produced aging is a reliable simulation. Some initial results are positive. If more comprehensive experiments confirm this trend, then it should be possible in a few hours to simulate accurately many years of aging in neutron tube targets; and that capability will be an extremely valuable tool for investigating designs of long-life tubes.

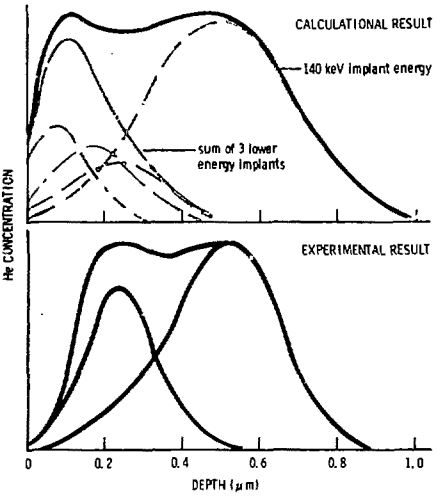

Fig. 5. We are conducting studies to determine if aging of neutron generator targets can be simulated by tailoring the distribution of implanted helium. The upper plot shows a nearly uniform depth profile that is achieved over an extended distance by combining single energy implants. The lower plot shows the results of three independent measurements that confirm the predicted uniformity.

We have determined how to increase the radiation tolerance of CMOS integrated circuits by orders of magnitude.

Radiation-hardened CMOS integrated circuits

The logical operation of many components in our nuclear weapons relies heavily on integrated circuit (IC) technology. In these applications, as well as in many others, it is usually a requirement that the electronic logic remain flawless following exposure to a radiation environment. Radiation sources may be either external (e.g., space radiation or nuclear bursts) or internal (e.g., electron-beam sources in vidicon tubes). Even IC fabrication steps, such as electron-beam metallization or plasma sputtering, can cause radiation damage.

Our primary effort has been to develop radiation-tolerant (hardened) IC components for use in nuclear weapon systems. Moreover, this hardening technology is equally applicable to electronics used in spacecraft or indeed to any electronic equipment that might be subjected to long-term, low-level radiation environments or to high-level accidental exposures.

Of the several IC technologies available, we have chosen to develop circuits based on the complementary-metal-oxide-semiconductor (CMOS) technology (Fig. 1). Two principal reasons for this choice are:

- The CMOS structure is inherently tolerant to neutron irradiation levels that exceed requirements for most applications.
- The CMOS planar technology is one of the most advanced large-scale-integrated (LSI) technologies available today. Complex LSI circuits can be rapidly designed and reliably fabricated by using computer-aided design plus libraries of standard configurations for circuit layout of basic logic functions.

Until recently doses of less than 100 Gy (Si)* would often cause failure of integrated circuits because the CMOS transistors had such low tolerance for ionizing radiation. In the past 2 years, however, we have demonstrated production of CMOS circuits that operate properly after doses of 10^6 Gy (Si) of ^{60}Co radiation. This improvement in hardness was accomplished by combined experimental and theoretical programs to determine the critical design and process parameters. Over 40 separate process-parameter dependences involving hundreds of processing variations have been investigated, and well over a thousand silicon wafers have been irradiated and measured to determine the effects of the exposure. In addition, fundamental studies and theoretical models have contributed substantially to understanding and controlling the basic degradation mechanisms.

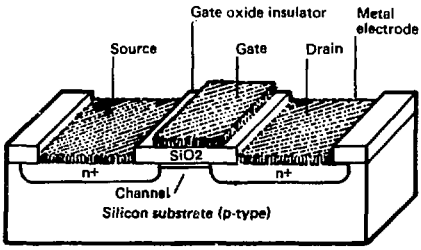

Fig. 1 A CMOS integrated circuit consists of n-channel and p-channel MOS transistors combined on the same substrate. For simplicity, only the n-channel transistor is shown. The formation of a minority carrier channel that controls the on-off state of the switch is highly dependent upon the magnitude of the electric field at the Si-SiO_2 interface.

Other problems addressed by Sandia studies but not discussed here include the effects of transient photocurrents in the semiconductor substrate, details of radiation-induced surface states at the Si-SiO_2 interface, and permanent physical damage to the active semiconductor regions. In this article we concentrate on a vulnerability due to the presence of hole-trapping sites in the gate oxide layer.

Basic Radiation Vulnerability

Irradiation of a CMOS transistor with neutrons alone will degrade the minority carrier lifetime in the silicon substrate, but the transistor is quite insensitive to this degradation. However, ionizing radiation, such as gamma rays

*The unit of absorbed dose is the gray (Gy): 1 Gy = 100 rad = 1 J/kg.

For further information about this article contact G. F. Derbenwick or R. C. Hughes.

or high-energy electrons, will produce free holes and electrons in the SiO_2 gate insulating layer. Some of the holes (but not usually the electrons) become trapped and create an electric field at the gate interface, thereby causing a shift in the turn-on voltage to more negative values. If the turn-on voltage of the n-channel transistor becomes zero or negative, the transistor locks in the "on" state and the logic circuit fails. Since holes trapped in the insulator are the source of the electric field that can lead to circuit failure, it is clear that the key to hardening CMOS devices is to prevent introduction of traps in the SiO_2 layer that can permanently trap holes.

Radiation-Hardened CMOS Circuits

Many of the processing steps used by manufacturers for the production of reliable, inexpensive CMOS circuits unfortunately also introduce many deep hole traps in the oxide; even the best commercial devices have been very sensitive to radiation charging. As part of our program for radiation hardening of microelectronics, we undertook the study of processing and design parameters that affect the hardness of the circuit. Of the large number of parameters investigated, three of the most important are oxide gate-insulator thickness, oxidation temperature, and postoxidation annealing temperature.

Oxide Thickness. A most significant observation made in the process-optimization study was that a CMOS device with a thinner oxide layer is invariably harder than one with a thicker oxide layer. There are three ways in which the oxide thickness influences hardness:

- A thin oxide has a smaller volume, and the number of holes created by a given penetrating radiation dose is smaller.
- The higher capacitance associated with a thinner oxide requires a larger number of trapped holes to produce the same voltage shift that would result in a thicker oxide.
- It has been observed, for the Sandia fabrication sequence, that the number of hole traps scales with the oxide thickness.

Thus, the effects of geometry and fabrication combine to reduce sharply the radiation-induced voltage shift for a given exposure when the oxide layer is made thinner (Fig. 2). Requirements for reliability and production yield, however, restrict the reduction of oxide thickness. Our program addresses optimization of the tradeoffs among reliability, yield, and hardness that must be effected in the fabrication of radiation-hardened CMOS devices.

Oxidation and Anneal Temperatures. Device hardness has also been observed to be strongly dependent upon oxidation temperature and the postoxidation annealing temperature. Gate oxides are thermally grown on silicon in dry oxygen at elevated temperatures. A postoxidation anneal, normally in a nitrogen atmosphere, is then necessary to gain proper control of the preirradiation turn-on voltage. Our measurements show that 1000°C is a near-optimum oxidation temperature, since device hardness is

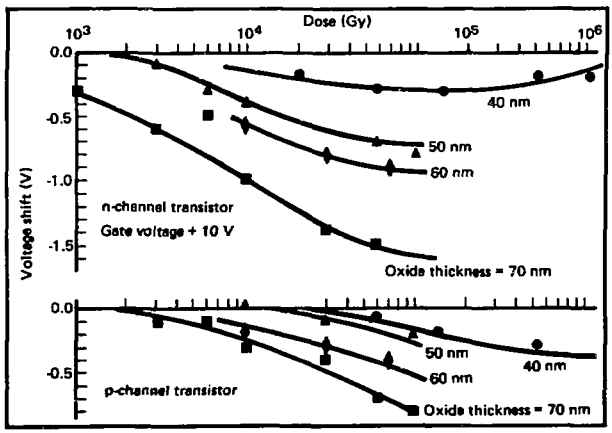

Fig. 2 The shift in turn-on voltage produced by a given radiation dose is reduced as the oxide layer is made thinner. Smaller voltage shifts imply harder devices. For a turn-on voltage of 2 V all these devices survive radiation exposures that are orders of magnitude greater than earlier commercial devices could tolerate.

degraded for other oxidation temperatures (Fig. 3). Device hardness is also degraded significantly for annealing temperatures above about 925°C (Fig. 4). Radiation-tolerance goals dictate annealing temperatures below 925°C, but low-temperature anneals are not so effective as high-temperature anneals for controlling preirradiation turn-on voltages. Our program has provided data for assessing these tradeoffs.

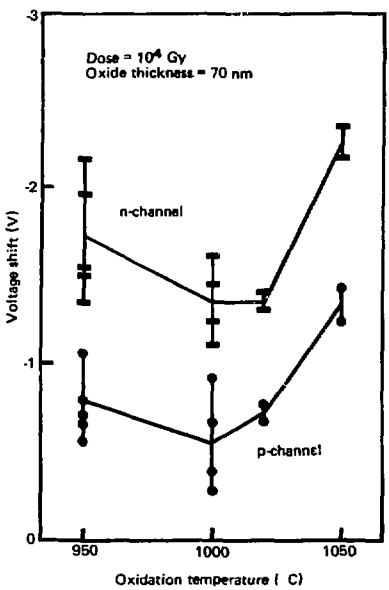

Fig. 3 Radiation-induced voltage shifts are minimized if the gate oxide layer is grown at a temperature of about 1000°C.

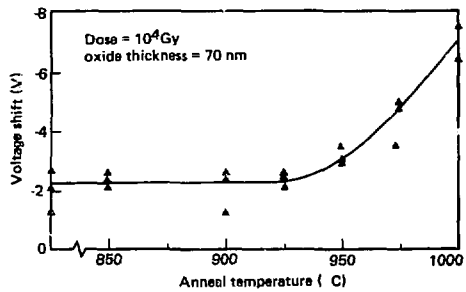

Fig. 4 Radiation hardness is degraded if the postoxidation anneal temperature is greater than about 925°C.

Conclusion

Electronic circuits that operate properly after exposure to ionizing radiation are necessary for nuclear weapon systems, satellites, and apparatus designed for use in radiation environments. Our program to develop and theoretically model radiation-tolerant integrated circuit components has resulted in devices that show an improvement in hardness up to a factor of ten thousand over earlier devices. An inverter circuit we produced functions properly after an exposure of 10^6 Gy (Si) which, as far as we know, is the record for an integrated circuit.

METRICATION

The International System of Units (SI) is a modernized metric system that is the world's common language for expressing scientific and technical data. It is a coherent system that uses seven base units. metre (m) for length, kilogram (kg) for mass, second (s) for time, kelvin (K) for thermodynamic temperature, ampere (A) for electric current, mole (mol) for amount of substance, and candela (cd) for luminous intensity. Two supplementary units are defined: radian (rad) for plane angle and steradian (sr) for solid angle. Many derived units are defined from the base and supplementary units. These include newton (force), joule (energy, work), pascal (pressure, stress), hertz (frequency), watt (power), and many electrical and photometric units. Below are conversion factors for quantities of special interest. Exact equivalences are marked with an asterisk (*); all other conversions are given to four significant figures.

LENGTH	1 m	= 3.281 ft = 39.37 in.
	1 mm	= 39.37 mils
	1 nm	= 10 A*
	1 km	= 0.6214 mi
MASS	1 kg	= 2.205 lbm
	1 Mg	= 1 tonne* = 1.102 tons (short, 2000 lbm)
FORCE	1 N	= 0.2248 lbf
ENERGY	1 J	= 0.2388 cal
	1 kJ	= 0.9478 Btu
	1 MJ	= 0.2778 kWh
	1 TJ	= 0.2381 kilotons (nuclear equivalent of TNT)
	1 fJ	= 0.6241 keV
PRESSURE	1 kPa	= 0.1450 psi
and		= 0.7501 torr
STRESS	1 MPa	= 10 bar* = 9.869 atmospheres
POWER	1 kW	= 1.341 hp = 737.6 ft-lbf/s
VOLUME	1 m^3	= 1.308 yd^3 = 35.31 ft^3
	1 L	= 1.057 qt (liquid)
DENSITY	1 kg/m^3	= 0.06243 lbm/ft^3
RADIATION	1 GBq	= 10^9 becquerels* = 10^9 disintegrations/s* = 0.02703 Ci
UNITS	1 kGy	= 10^3 grays* = 10^3 J/kg* = 10^5 rad* = 0.2388 cal/g

SI includes a set of prefixes that can be combined with the names of the units to indicate multiples and submultiples.

E(exa)	$= 10^{18}$	**M**(mega)	$= 10^{6}$	**n**(nano)	$= 10^{-9}$
P(peta)	$= 10^{15}$	**k**(kilo)	$= 10^{3}$	**p**(pico)	$= 10^{-12}$
T(tera)	$= 10^{12}$	**m**(milli)	$= 10^{-3}$	**f**(femto)	$= 10^{-15}$
G(giga)	$= 10^{9}$	μ(micro)	$= 10^{-6}$	**a**(atto)	$= 10^{-18}$

The use of c(centi) for 10^{-2}, although allowed in SI, is discouraged.